On the Coordination of Electric Water Heater Loads for Frequency Support and Load Following in Power Systems

*

1st Amirali Delavaran Shiraz
dept. of Electrical Engineering
Ecole Polytechnique de Montréal
Montréal, Canada
amirali.delavaran-shiraz@polymtl.ca

2nd Roland Malhamé
dept. of Electrical Engineering
Ecole Polytechnique de Montréal
Montréal, Canada
roland.malhame@polymtl.ca

***Abstract*—This paper investigates the potential of Electric Water Heater (EWH) equipped with droop control mechanism to provide decentralized load-side frequency support in modern power systems. Leveraging the inherent flexibility and thermal inertia of EWHs, a stochastic model based on Partial Differential Equation (PDE) is developed to analyze their aggregate behavior under Demand Response (DR) scenarios. Numerical simulations demonstrate the efficacy of the proposed control mechanism in mitigating different types of frequency oscillations, ensuring grid stability, and reducing reliance on conventional generators. Results show a significant improvement in system performance, compared to systems without EWH-based DR. These findings highlight the viability of EWHs as a robust and scalable tool for grid frequency stabilization while maintaining consumer comfort.**

***Index Terms*—Frequency stability, Demand Response, Electric Water Heaters, Droop control, Kolmogorov equations, Partial Differential Equations, Primary Frequency Regulation.**

I. Introduction

Droop control has historically been a successful approach for mitigating frequency fluctuations in power systems, particularly in synchronous machines. The simplicity and decentralized nature of droop control allow each generator to autonomously adjust its output in response to frequency deviations, based on local signals. This method ensures that each generator contributes proportionally to its capacity, provided that it does not exceed its generation limits [1]. The advantage of this mechanism lies in its reliance on the universally observed system frequency to manage power generation without the need for centralized coordination.

In the current era, where renewable energy sources such as solar and wind are increasingly integrated into power grids, the supply side is becoming more unpredictable. This growing intermittency in energy generation has highlighted the importance of involving both the supply and demand sides in the effort to stabilize grid frequency and voltage. While this concept was initially introduced by Schweppe through homeostatic control [2], it has gained renewed attention in the context of power electronics, especially with the advent of the virtual synchronous machine proposed by Zhong [3]. These electronically achievable synchronous dynamics are essential in modern grids, but not all loads are equally suited to support frequency control.

Among the various types of electrical loads, EWHs stand out as a class of devices capable of providing significant flexibility. Unlike inflexible loads such as lamps or washing machines, EWHs can be adjusted to provide demand-side support for frequency stabilization [4]–[7] and they also consume relatively high amounts of power. It is estimated that EWHs consume about a third of the energy consumed by households [8].

Due to their thermal inertia and reliance on simple resistive heating elements, EWHs are well-suited for integration into droop control schemes without compromising user comfort [9]. Furthermore, EWHs can store thermal energy and respond dynamically to grid conditions, acting both as flexible loads and energy storage devices.

In this study, we explore how a droop-based control mechanism, as a decentralized system, can be applied to a large collection of EWHs. Decentralized droop control has become a promising strategy for regulating grid frequency. Unlike centralized control schemes, which require significant communication infrastructure and can suffer from delays, droop control operates locally. Each device autonomously adjusts its power output or consumption based on the locally measured frequency deviation. This approach enables faster response times, improves the robustness of the system, and ensures scalability, making it ideal for modern power systems with high variability [3], [10].

The proposed system aims to allow EWHs to contribute to frequency stabilization, not only for minor frequency fluctuations but also for more significant deviations caused by generation deficits or surpluses. Since EWHs are controlled by thermostats, only those that are actively heating at any given time can participate in frequency regulation. This stochastic

behavior, driven by hot water consumption patterns, varies by time of day and week [11], and must be accounted for in the control strategy.

To address these challenges, we develop a model based on PDEs that characterizes the aggregate behavior of droop-controlled EWHs. This model is coupled with a simplified power system incorporating conventional synchronous generators, enabling us to test the effectiveness of EWHs in supporting grid frequency and alleviating the burden on traditional generators. Through numerical simulations, we assess the ability of EWHs to contribute to frequency control under both normal operating conditions and during times of grid stress.

The rest of the paper is organized as follows: Section II provides an in-depth description of the system model, including the integration of EWHs into a simplified power system. Section III introduces the stochastic modeling framework for EWHs, incorporating hybrid-state Markov processes and PDEs to characterize their individual and aggregate behavior. This section details the formulation of transition probabilities, thermostat dynamics, and energy extraction rates. Section IV presents the simulation framework, describing the numerical methods employed, including the Lax-Wendroff scheme for solving the PDEs and the Monte Carlo approach for validation. Section V discusses the simulation results, highlighting the impact of EWH-based demand response on frequency stabilization under different grid conditions. The results are analyzed in terms of frequency deviations, power consumption adjustments, and response times, demonstrating the efficacy of the proposed approach. Finally, Section VI concludes the paper by summarizing the key findings, discussing limitations, and offering recommendations for future research.

II. Power System and Control

A. System Overview

To study the interaction between EWHs and traditional power systems, we developed a simplified control area model. This system includes a non-reheat steam turbine generator and synchronous machines that provide Primary Frequency Regulation (PFR). The generator operates using a standard droop control scheme, which adjusts output in response to frequency deviations [1]. A block diagram of this model is shown in Fig. 1, with the parameters describing the dynamics of the power system. $\Delta\omega$, represents the angular velocity deviation of the generator rotors, is directly related to the system frequency deviation, Δf, by $\Delta\omega = 2\pi\Delta f$, where f is the system frequency in Hz. P_e^0 is the load reference, P_g is the generated power adjusted dynamically, and P_d is the total power demand. P_{DR} refers to power contributed by DR resources.

The time constants T_{ch} and T_G reflect delays in turbine response, with T_{ch} for steam flow and T_G for governor adjustments. The inertia constant, M, dampens frequency changes, while the droop constant, R, governs proportional adjustments in generator output. The load damping factor, D, generally assumed to be 1 p.u., indicates that a 1% frequency change results in a corresponding 1% change in load.

These parameters collectively influence the system's ability to maintain stability and integrate flexible resources like EWHs.

The main goal of this system is to balance electricity generation and demand while keeping the frequency within acceptable limits. Under normal conditions, load changes are managed by adjusting the generator's mechanical power. However, as renewable energy sources like wind and solar add variability to the supply side, demand-side resources like EWHs are becoming increasingly important for maintaining system stability.

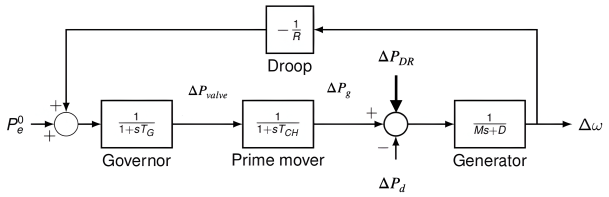

Fig. 1. Block diagram of the simplified power system, integrating EWHs for frequency regulation.

B. Frequency Response and the Swing Equation

The system's frequency dynamics can be described using the well-known Swing Equation [1], which relates frequency deviations to the imbalance between mechanical and electrical power:

$$\frac{d\Delta f(t)}{dt} = \frac{\Delta P_m(t) - \Delta P_e(t)}{M} - D\Delta f(t), \tag{1}$$

where:

- $\Delta P_m(t)$: Mechanical power change,
- $\Delta P_e(t)$: Electrical power change.

This equation captures the fundamental interplay between inertia, damping, and power imbalances in the system. The term $\frac{\Delta P_m(t) - \Delta P_e(t)}{2H}$ represents the acceleration or deceleration caused by power imbalances, while $-D\Delta f(t)$ accounts for the damping effect, which naturally opposes frequency deviations. These dynamics are central to understanding and designing demand-side frequency regulation strategies, such as the droop-based control of Electric Water Heaters (EWHs) proposed in this study.

C. Droop-Based Control Strategy for EWHs

EWHs in this study, are integrated into the system through a droop-based control mechanism that dynamically adjusts their power consumption in response to frequency changes. Specifically, when the frequency of the grid deviates from its nominal value, the power consumption of the individual EWHs is modulated according to the following equation:

$$P_{\text{EWH}}(t) = P_{\text{nom}} \left(1 + \frac{\Delta f(t)}{K}\right), \tag{2}$$

where $P_{\text{EWH}}(t)$ is the instantaneous power consumption of the EWH, P_{nom} is the nominal power consumption, $\Delta f(t)$ is the deviation in frequency from its nominal value, and K is the droop constant. The droop constant determines the sensitivity of power adjustments to frequency deviations.

The control mechanism operates as follows:

- When grid frequency decreases due to generation shortfalls, EWHs proportionally reduce their power consumption, alleviating the stress on the grid.
- Conversely, when the frequency increases due to excess generation, EWHs can increase their power consumption, absorbing the surplus energy.

This decentralized control ensures that each EWH autonomously adjusts its operation without requiring real-time communication or centralized coordination.

D. Challenges and Key Considerations

While the decentralized nature of droop control simplifies the integration of EWHs, it also presents unique challenges. EWHs only contribute to frequency control when they are actively heating, and this behavior depends on user-driven hot water consumption patterns. These patterns vary by time of day and can affect the overall response of the system [12]. Addressing this variability requires a control strategy that accounts for the stochastic nature of EWH operation.

III. Stochastic Modeling of Electric Water Heaters

This section presents a detailed stochastic model for individual and aggregated EWHs under frequency control, utilizing PDEs to capture their dynamic behavior. The model incorporates thermostat deadbands, droop regulation, and aggregate dynamics, enabling an analysis of their potential in DR scenarios.

A. Assumptions and System Description

The model assumes a homogeneous population of EWHs with fixed physical parameters:

- Rated power consumption $R = 4.5\,\text{kW}$,
- Thermostat deadband $[T_-, T_+]$,
- Ambient temperature T_a.

The EWHs are divided into ON and OFF states, controlled by thermostatic switching and droop regulation, which dynamically adjusts power consumption based on system frequency deviations.

B. Markov Chain Modeling of EWH

The stochastic operation of EWH can be effectively described using a hybrid-state Markov chain. This approach models the probabilistic transitions between ON and OFF states of EWH, driven by thermostat control, user demand, and external grid signals such as frequency deviations.

a) State Definition:: The i-th EWH is characterized by a state $m(t) = (s)$, where:

- s: Operational state of the EWH, with $s = 1$ for ON (heating) and $s = 0$ for OFF (cooling).

b) Transition Dynamics:: Furthermore, the two-state Markov chain $q(t)$ is characterized by the (interval-wise) time-invariant transition rates α_0 and α_1. The switching probabilities are governed by the following equations:

$$Pr(q(t+h) > 0 \mid q(t) = 0) = \alpha_1 h + o(h), \quad (3)$$

$$Pr(q(t+h) = 0 \mid q(t) > 0) = \alpha_0 h + o(h), \quad (4)$$

where:

α_1 : Transition rate from state 0 to state 1,

α_0 : Transition rate from state 1 to state 0,

h : Time increment (small step),

$o(h)$: Higher-order terms negligible as $h \to 0$.

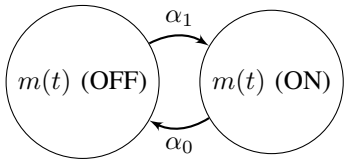

Fig. 2. Markov chain representation of EWH transitions. S_0: OFF state, S_1: ON state. Transitions occur based on the time-invariant transition rates α_0 and α_1.

The Markov chain model, which has also been illustrated in Fig. 2 provides a probabilistic framework to analyze the aggregated behavior of EWH. It enables accurate predictions of their contributions to grid stability by taking into account the temperature dynamics, user demand, and control signals.

C. The Coupled Fokker-Planck Equations for Aggregate EWH Modeling

The operation of EWH as controllable loads for demand response involves the modeling of both individual and aggregate behavior. This section outlines the process of deriving aggregate load dynamics from individual behavior and the corresponding partial differential equations.

1) Establishing a Model for Individual and Aggregate Loads: The operation of an individual EWH is governed by its physical parameters and thermostat control logic. The following simplified dynamic equation describes the evolution of the temperature within the water tank during operation [12]. The model assumes a constant rate of energy extraction when hot water demand is ON:

a) Simplified EWH Dynamic Equation::

$$\frac{d\lambda}{dt} = -a(\lambda - T_a) + Rm_t(t) - A(t), \quad (5)$$

where:

- λ: Water temperature inside the tank,
- T_a: Ambient temperature,
- a: Heat loss coefficient due to thermal dissipation,
- R: Heating power rate when the EWH is ON,
- $A(t)$: Rate of energy extraction due to hot water demand.
- $m_t(t)$: Thermostat control boolean.

When hot water demand is ON, the energy extraction rate $A(t)$ significantly influences the temperature evolution. The extraction process cools the water, causing the temperature λ to decrease. If λ falls below the lower thermostat limit T_-, the heater is activated to restore the temperature within the deadband $[T_-, T_+]$. A detailed explanation of how these parameters are being calculated is provided in Appendix A.

b) Total Power Consumption of a Population of EWHs:: In the context of a homogeneous control group consisting of M EWH, all devices are assumed to share identical statistics and parameters. The total electricity demand of the M devices at time t is expressed as:

$$P(t) = R' \sum_{i=1}^{M} m_i(t), \tag{6}$$

where:

- R': power rating of the heating element (Watts).
- $P(t)$: Total power demanded by the group at time t.
- $m_i(t)$: Binary state of the i-th EWH ($m_i(t) = 1$ when ON, $m_i(t) = 0$ when OFF).

However, $P(t)$ is a highly stochastic quantity due to the variability of individual EWH operations. To simplify the analysis, the empirical mean $\bar{m}(t)$ is considered, representing the average fraction of ON-state devices. Under the assumption of independent EWH states, $\bar{m}(t)$ converges to the expected value of a generic $m_i(t)$ as $M \to \infty$, due to the strong law of large numbers:

$$\bar{m}(t) \triangleq \frac{1}{M} \sum_{i=1}^{M} m_i(t) \quad \underrightarrow{a.e.} \quad E_w[m(t)], \tag{7}$$

where:

- $\bar{m}(t)$: Aggregate operating state, representing the average fraction of ON-state devices in the group.
- $E_w[m(t)]$: Expected value of $m(t)$, conditional on environmental factors such as ambient temperature T_a.

In the homogeneous case, $P(t)$ is proportional to $\bar{m}(t)$. This aggregation simplifies the representation of power consumption for large populations of EWHs.

2) Partial Differential Equations of Load Dynamics: The load dynamics of a homogeneous group of EWHs can be modeled by the evolution of Probability Density Function (PDF)s describing the thermostat states. Consider the hybrid-state Markov process:

$$\begin{bmatrix} T(t) \\ m(t) \\ q(t) \end{bmatrix},$$

where $T(t)$ is the water temperature, $m(t)$ is the thermostat binary state, and $q(t)$ represents the water extraction state. The joint PDF s can be expressed as:

$$f_{ij}(\lambda, t)d\lambda = P[\lambda \leq T(t) \leq \lambda + d\lambda, m(t) = i, q(t) = j], \tag{8}$$

where $i, j \in \{0, 1\}$. These PDF s provide a basis for understanding the aggregate behavior of EWHs under varying operational states.

Following Malhamé's framework [12], the hybrid-state PDFs f_{ij} satisfy the following coupled PDEs:

$$\frac{\partial f_{11}(\lambda,t)}{\partial t} = -\frac{\partial}{\partial \lambda}\left[r_{11}(\lambda,t) f_{11}(\lambda,t)\right] - \alpha_1 f_{11}(\lambda,t) + \alpha_0 f_{10}(\lambda,t), \tag{9}$$

$$\frac{\partial f_{10}(\lambda,t)}{\partial t} = -\frac{\partial}{\partial \lambda}\left[r_{10}(\lambda,t) f_{10}(\lambda,t)\right] + \alpha_1 f_{11}(\lambda,t) - \alpha_0 f_{10}(\lambda,t), \tag{10}$$

$$\frac{\partial f_{01}(\lambda,t)}{\partial t} = -\frac{\partial}{\partial \lambda}\left[r_{01}(\lambda,t) f_{01}(\lambda,t)\right] - \alpha_1 f_{01}(\lambda,t) + \alpha_0 f_{00}(\lambda,t), \tag{11}$$

$$\frac{\partial f_{00}(\lambda,t)}{\partial t} = -\frac{\partial}{\partial \lambda}\left[r_{00}(\lambda,t) f_{00}(\lambda,t)\right] + \alpha_1 f_{01}(\lambda,t) - \alpha_0 f_{00}(\lambda,t). \tag{12}$$

Here, the terms $r_{ij}(\lambda, t)$ represent the water cooling rates under different operational states:

$$r_{11}(\lambda,t) \triangleq a(\lambda - T_a) - R + A(t), \tag{13}$$

$$r_{10}(\lambda,t) \triangleq a(\lambda - T_a) - R, \tag{14}$$

$$r_{01}(\lambda,t) \triangleq a(\lambda - T_a), \tag{15}$$

$$r_{00}(\lambda,t) \triangleq a(\lambda - T_a) + A(t). \tag{16}$$

Physical Interpretation of r_{ij}:

- $r_{11}(\lambda, t)$: Cooling rate of the water when the EWH is ON and facing a water demand.
- $r_{10}(\lambda, t)$: Cooling rate when the EWH is ON and not facing a water demand.
- $r_{01}(\lambda, t)$: Cooling rate when the EWH is OFF and facing a water demand.
- $r_{00}(\lambda, t)$: Cooling rate when the EWH is OFF and not facing a water demand.

By solving these coupled PDEs, the aggregate dynamics of the EWH group can be derived, providing insights into the system's behavior under varying conditions.

3) Boundary Conditions: The boundary conditions ensure conservation of probability and realistic behavior and must hold for all t:

1) **Conditions at infinity ($\lambda \to \pm\infty$):**

$$f_{11}(-\infty, t) = f_{10}(-\infty, t) = 0 \tag{17}$$

2) **Probability conservation:**

a) At T_-, for $j = 0, 1$:

$$-r_{1j}(T_-,t) f^a_{1j}(T_-,t) + r_{1j}(T_-,t) f^b_{1j}(T_-,t) + r_{0j}(T_-,t) f^b_{0j}(T_-,t) = 0 \tag{18}$$

b) At T_+, for $j = 0, 1$:

$$r_{1j}(T_+,t) f^b_{1j}(T_+,t) + r_{0j}(T_+,t) f^b_{0j}(T_+,t) = 0 \tag{19}$$

3) **Absorbing boundaries:**

a) At T_+, for $j = 0, 1$:

$$0 \leq -r_{1j}(T_+,t) f_{1j}(T_+,t) \tag{20}$$

b) At T_-, for $j = 0, 1$:

$$0 \leq r_{0j}(T_-, t) f_{0j}(T_-, t) \tag{21}$$

The boundary conditions defined above exhibit an important characteristic. Although most conditions are automatically satisfied, an exception occurs for absorbing boundaries. Specifically, when $r_{11}(T_+, t)$ is positive, $f_{11}(T_+, t)$ must be zero, as indicated by equation (20). This is because f_{11}, being a probability density function, cannot become negative. The situation $0 \leq r_{11}(T_+, t)$ arises when the power of the heating element is lower than the power loss associated with the extraction of hot water under $q(t) = 1$.

4) Aggregate Behavior: Finally, the fraction of devices in the ON state is given by:

$$\bar{m}(t) = \mathbb{E}_w[m(t)] = \int_{-\infty}^{\infty} [f_{11}(T, t) + f_{10}(T, t)]\, dT \tag{22}$$

This integral provides the expected value of the operating state, contributing to an understanding of aggregate system behavior.

These boundary conditions, coupled with the Fokker-Planck equations described earlier, facilitate the derivation of PDFs related to temperature distributions across various thermostatic states, as illustrated in Fig. 3. This PDF figure highlights two zones: Zone a spans from $-\infty$ to T_-, representing the region where temperatures are below the thermostat's activation threshold, primarily describing cooling states. Zone b extends from T_- to T_+, capturing the thermostat's deadband where the EWH switches between ON and OFF states. These zones reflect the interplay between cooling, heating, and stochastic transitions within the system.

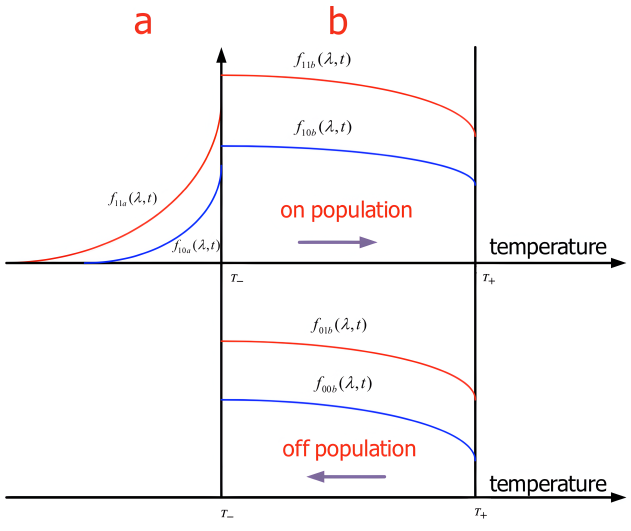

Fig. 3. Illustration of dynamical system (9) to (12). T_- and T_+ are lower and upper edges of the thermostats deadbands.

D. Summary of Insights

This mathematical framework demonstrates the potential of EWHs for rapid, decentralized primary frequency regulation. By combining thermostat control, droop mechanisms, and aggregated dynamics, the proposed model effectively characterizes EWH contributions to grid stability.

IV. Simulation Framework

To evaluate the system, we built a simulation combining deterministic generator dynamics with the stochastic behavior of EWHs. The frequency response in (1) and the EWH droop behavior in (2) were iteratively solved to analyze system performance. Simulations were performed under various operating conditions to compare the effectiveness of EWH integration against traditional PFR-only systems.

A. Simulation Assumptions

The simulation assumes a homogeneous population of EWHs with the following characteristics, with corresponding tables summarizing the values used as default parameters for the simulations:

- Fixed physical parameters, including a thermostat deadband between T_- and T_+, and an ambient temperature of $T_a = 22°\text{C}$. These values are summarized in Table I.
- In our simulations, the EWH operate at a default heating rate of $\frac{2R}{3} = 3KW$, with power adjustments governed by a droop-based mechanism. The power output is bounded by a minimum threshold of $\frac{R}{3} = 1.5KW$ and a maximum threshold of $R = 4.5KW$, ensuring sufficient energy reserves for grid stability and customer comfort. These thresholds allow the EWH to respond promptly to frequency deviations while maintaining adequate thermal storage. Adjustments to the heating rate are proportional to the frequency deviation ($\Delta f(t)$), as detailed in Algorithm 1.
- Hot water consumption patterns modeled as a stochastic process, governed by Markov chain transitions between ON and OFF states, fully explain in Appendix A. Table II provides the values used for the Markov chain parameters and energy extraction rates.
- A simplified representation of grid dynamics that accounts for frequency deviations caused by supply-demand imbalances, as detailed in Section II. The generator parameters, including the droop constant R and inertia constant M, are set to emulate realistic system behavior. Notably, the generator's PFR is designed to handle frequency deviations by adjusting the mechanical power within strict limits, ensuring that it can compensate for only up to 10% of the nominal power deviation. This means that for power deviations of $\pm 10\%$ of the nominal power, the generator output is capped to regulate the frequency effectively. The corresponding power system parameters are summarized in Table III.

B. Numerical Methods

To accurately simulate the system dynamics, we use a combination of numerical methods.

Algorithm 1: Update_HeatingRate

Input : $\Delta f(t)$, R, K
Output: R_{new}
if $\Delta f(t) < -K$ **then**
  $R_{new} = R/3$
else if $\Delta f(t) > K$ **then**
  $R_{new} = R$
else
  $R_{new} = \frac{2R}{3} + \frac{\Delta f}{K} \cdot \frac{R}{3}$

TABLE I
EWH PARAMETERS

Parameter	Description	Value
R (kW)	Rated power consumption	4.5
U ($\frac{\text{J}}{\text{min}\cdot^\circ\text{C}\cdot\text{m}^2}$)	Thermal conductivity	8.75
A_r (m^2)	Surface area of tank insulation	2.8
Thermostat Dead-Band (°C)	Operating temperature range	60–65
T_a (°C)	Ambient temperature	22
M (kg)	Mass of water in the tank	304

- Markov chain models capture the stochastic transitions between ON and OFF states of EWHs, driven by thermostat controls, user demand, and external frequency signals.
- PDEs are used to describe how the aggregate behavior of EWHs responds to frequency regulation, modeling their contribution to grid stability.
- The Lax-Wendroff method is applied to solve the Kolmogorov equations that govern the evolution of probability densities. This ensures an accurate and stable representation of how aggregated devices interact with the grid over time.

1) Discretization of the Markov Chains: The discretization of the Markov chain is based on the continuous-time formulation provided earlier. The population distribution vector of the Markov chain at time t, $N(t)$, evolves according to:

$$\frac{dN}{dt} = BN(t). \tag{23}$$

Using a sampled version of $N(t)$ at a fixed time step Δt, the discretized form can be written as:

$$N(t + \Delta t) = e^{\Delta t B} N(t). \tag{24}$$

For small Δt and assuming small values for B, we can use a first-order approximation:

$$e^{\Delta t B} \approx \mathbb{I}_4 + \Delta t B, \tag{25}$$

where $\mathbb{I}_4$ is the identity matrix of size 4. This leads to the discrete-time approximation of the continuous-time Markov chain transition probabilities:

$$\begin{aligned} Pr(q(t + \Delta t) > 0 | q(t) = 0) &= \alpha_1 \Delta t, \\ Pr(q(t + \Delta t) = 0 | q(t) > 0) &= \alpha_0 \Delta t. \end{aligned} \tag{26}$$

This formulation provides a numerically efficient way to simulate the transitions between the ON and OFF states of the EWHs while maintaining fidelity to the underlying continuous-time dynamics.

TABLE II
HOT WATER CONSUMPTION PATTERNS AND PARAMETERS

Parameter	Value
A (°C/min)	0.81
a (1/min)	0.193×10^{-4}
α_0 (min^{-1})	0.042
α_1 (min^{-1})	0.52

TABLE III
POWER SYSTEM PARAMETERS

Parameter (Units)	Description	Value
T_{ch} (s)	Steam Chest Time Constant	0.3
T_G (s)	Governor Time Constant	0.2
M (s)	Generator's Inertia Constant	10
R_{GD} (pu)	Generator's Droop Constant	0.05
D (pu)	Load Damping Factor	1

2) Numerical Solution Using the Lax-Wendroff Method: The probability density functions $f_{ij}(x,t)$ evolve according to the coupled partial differential equations (9)-(12). These can be expressed compactly as follows:

$$\frac{\partial}{\partial t} f(x,t) = \frac{\partial}{\partial x}[A(x,t) f(x,t)] + B f(x,t), \tag{27}$$

where $A(x,t)$ is the cooling rate matrix, and B is the transition matrix associated with the Markov chain. These matrices are defined as:

$$f(x,t) = \begin{bmatrix} f_{00}(x,t) \\ f_{01}(x,t) \\ f_{10}(x,t) \\ f_{11}(x,t) \end{bmatrix}, \tag{28}$$

$$A(x,t) = \begin{bmatrix} r_{00}(x) & 0 & 0 & 0 \\ 0 & r_{01}(x) & 0 & 0 \\ 0 & 0 & r_{10}(x,t) & 0 \\ 0 & 0 & 0 & r_{11}(x,t) \end{bmatrix}, \tag{29}$$

$$B = \begin{bmatrix} -\alpha_0 & \alpha_1 & 0 & 0 \\ \alpha_0 & -\alpha_1 & 0 & 0 \\ 0 & 0 & -\alpha_0 & \alpha_1 \\ 0 & 0 & \alpha_0 & -\alpha_1 \end{bmatrix}. \tag{30}$$

The cooling rates in the matrix $A(x,t)$ are treated as time independent in the numerical simulations because the only time-dependent factor, the water demand, is simplified by assuming a constant rate of energy extraction, as described in equations (13) to (15) and detailed in Appendix A. Similarly, the matrix B is considered time and temperature independent, as explained in Appendix A.

The numerical solution for the evolution equation in (27) is obtained using the Lax-Wendroff scheme. This scheme provides a second-order accurate approximation for both time

and space derivatives. The spatial derivatives are discretized as follows:

$$\frac{\partial f_m^n}{\partial x} = \frac{f_{m+1}^n - f_{m-1}^n}{2\Delta x}, \tag{31}$$

$$\frac{\partial^2 f_m^n}{\partial x^2} = \frac{f_{m+1}^n - 2f_m^n + f_{m-1}^n}{\Delta x^2}. \tag{32}$$

Using a second-order Taylor expansion, the Lax-Wendroff time-stepping formula is expressed as:

$$\begin{aligned} f_m^{n+1} = f_m^n + kaf_m^n + kA(x,t)\frac{\partial}{\partial x}f_m^n + kBf_m^n \\ + \frac{1}{2}k^2\left[3A_m^n a\frac{\partial f_m^n}{\partial x} + \frac{\partial}{\partial t}R^n\frac{\partial f_m^n}{\partial x}\right. \\ + {A_m^n}^2\frac{\partial^2 f_m^n}{\partial x^2} + A_m^n\frac{\partial B}{\partial x}f_m^n \\ + (A_m^n B + BA_m^n)\frac{\partial f_m^n}{\partial x} \\ \left. + (a)^2\frac{\partial f_m^n}{\partial x} + B(B+2a)\frac{\partial f_m^n}{\partial x}\right] \end{aligned} \tag{33}$$

where k is the time step size, Δx is the spatial grid size, A_m^n represents the cooling rate matrix, and B is the transition matrix.

3) Boundary Conditions: The boundary conditions for the numerical solution of the Kolmogorov equation ensure probability conservation, continuity, and proper behavior at boundaries and infinity.

Absorbing Boundaries:

At the upper temperature deadband T_+, for $j = 0, 1$:

$$f_{11}(T_+, t) = 0, \text{ if } r_{11}(T_+, t) \geq 0, \tag{34}$$

$$f_{10}(T_+, t + \Delta t) = -\frac{r_{10}(T_+, t)}{r_{00}(T_+, t)} f_{10}(T_+, t). \tag{35}$$

At the lower temperature deadband T_-, for $j = 0, 1$:

$$f_{00}(T_-, t + \Delta t) = f_{00}(T_-, t) - \frac{r_{00}(T_-, t)}{r_{10}(T_-, t)} f_{00}(T_-, t), \tag{36}$$

$$f_{11}(T_-, t + \Delta t) = f_{11}(T_-, t) - \frac{r_{01}(T_-, t)}{r_{11}(T_-, t)} f_{01}(T_-, t). \tag{37}$$

Probability Conservation:

At T_-, for $j = 0, 1$:

$$-r_{1j}(T_-, t) f_{1j}^a(T_-, t) + r_{1j}(T_-, t) f_{1j}^b(T_-, t) + \tag{38}$$

$$r_{0j}(T_-, t) f_{0j}^b(T_-, t) = 0. \tag{39}$$

At T_+, for $j = 0, 1$:

$$r_{1j}(T_+, t) f_{1j}^b(T_+, t) + r_{0j}(T_+, t) f_{0j}^b(T_+, t) = 0. \tag{40}$$

Conditions at Infinity:

As $T \to \pm\infty$:

$$f_{11}(-\infty, t) = 0, \quad f_{10}(-\infty, t) = 0. \tag{41}$$

These boundary conditions govern the numerical behavior at deadband limits, infinity, and ensure the model adheres to physical and probabilistic constraints.

4) Validation: To validate the accuracy of the evolution equations and the proposed numerical simulation method, we compared the results with those obtained from Monte Carlo simulations, as shown in Fig. 4. In this case, the Monte Carlo simulation used a sample size of 100,000 and demonstrated strong agreement with the behavior predicted by the Fokker-Planck simulation. As the sample size increases, this agreement is expected to improve further. However, it is important to note that Monte Carlo simulations require significantly more computational time compared to the finite-difference approximation employed in the PDE-based approach.

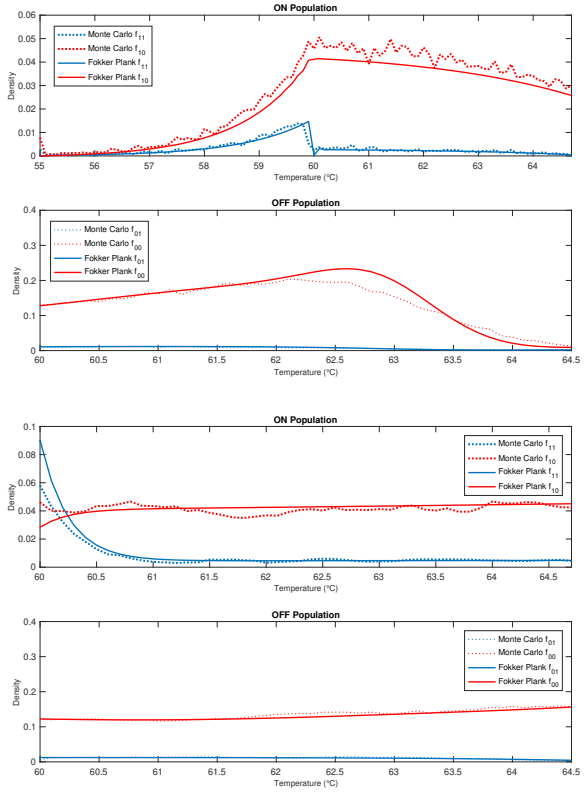

Fig. 4. ON and OFF state density functions calculated by Kolmogorov equations and Monte Carlo simulation for two cases: (Top) $A = 0.81\frac{^\circ C}{\text{min}}$, where $r_{11}(x_+, t) > 0$, and (Bottom) $A = 0.28\frac{^\circ C}{\text{min}}$, where $r_{11}(x_+, t) \leq 0$. These cases show how the system behaves as it reaches steady state under different conditions, confirming the accuracy of our numerical method.

By combining these methods, we achieve a detailed and realistic simulation of both individual EWHs and their collective impact on the power grid.

C. Simulation Scenarios

The following scenarios were explored to assess the system's performance:

- **Sudden Demand Changes**: Simulations of abrupt increases and decreases in demand (e.g., ± 0.015 p.u.) to evaluate the EWH response under different perturbation sizes.

- **Synthetic Real-Time Perturbations**: Use of Fourier-based synthetic load perturbations, constructed from real-world frequency data, to mimic practical grid conditions.
- **Time-Dependent Hot Water Demand**: Analysis of the temporal effects of varying hot water usage rates on the number of active EWHs and their contribution to demand response.

V. Results

This section presents the outcomes of the proposed approach, evaluating the efficacy of aggregated EWHs equipped with droop control mechanisms in providing primary frequency regulation. The results are based on simulations conducted under various scenarios, including sudden load changes and oscillatory frequency perturbations.

A. Frequency Stabilization under Sudden Load Changes

When the system experienced sudden load changes ranging from 0.015 p.u. to 0.1 p.u. at $t = 2$ min, the EWHs demonstrated a remarkable ability to stabilize grid frequency. As illustrated in the upper plot of Fig. 5, a disturbance of 0.015 p.u.—approximately half the total power consumption of the EWHs—was effectively managed. The system utilizing EWH-based DR maintained a steady-state frequency of 60.001 Hz, in contrast to 59.96 Hz when EWHs were not employed, relying solely on PFR. This highlights the capability of EWHs to provide robust support for primary frequency regulation.

Furthermore, the lower plot of Fig. 5 demonstrates the effectiveness of the DR strategy even under larger disturbances, up to three times the total power consumption of the EWHs. Despite these significant perturbations, the system with droop-controlled EWHs restored stability efficiently, underscoring their critical role in enhancing grid resilience.

B. Response to Oscillatory Perturbations

The performance of the proposed droop mechanism was evaluated under oscillatory perturbations, inspired by a frequency disturbance observed in Quebec [13]. As showed in the upper plot of Fig. 6, the EWHs effectively tracked frequency deviations while ensuring customer comfort. The middle plot highlights the sinusoidal variation in the total number of ON devices, showcasing the droop mechanism's ability to dynamically adjust power consumption for frequency regulation. The mean system frequency improved notably, from 60.018 Hz without EWHs to 60.006 Hz with EWHs, underscoring the capability of droop-controlled EWHs to mitigate oscillatory disturbances. Furthermore, the lower plot demonstrates how the use of EWHs and the droop control mechanism alleviates the burden on the generators, with the mean generator power remaining closer to 1 p.u., the nominal value. This reduction in generator adjustment effort is crucial for minimizing operational costs and mitigating delays.

C. Time-Dependent Performance

The effect of varying hot water demand on EWH performance was analyzed to assess its impact on DR capabilities.

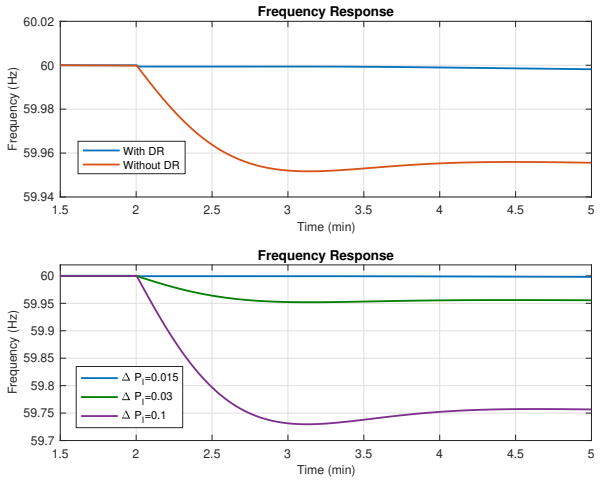

Fig. 5. Frequency response of the system under sudden load changes with and without EWH-based DR. The upper plot illustrates the system's performance under a 0.015 p.u. disturbance, where EWHs maintained a steady-state frequency of 60.001 Hz compared to 59.96 Hz without their involvement. The lower plot shows the system's resilience under larger disturbances, demonstrating the ability of droop-controlled EWHs to restore stability even when perturbations exceed three times their total power consumption.

During periods of high demand ($A = 0.81\,^{\circ}\mathrm{C/min}$ at 8 PM, as shown in Fig. 12), EWHs initially consumed approximately 0.03 p.u. and achieved a power reduction of 0.015 p.u. during a perturbation event of 0.015 p.u.

Conversely, during periods of low demand ($A = 0.32\,^{\circ}\mathrm{C/min}$, representing the average daily energy rate), the fraction of ON devices dropped significantly from 47.8% (high demand) to 14.8% (low demand). This reduction in ON devices resulted in a much lower aggregated power consumption of approximately 0.01 p.u., as shown in the middle and lower plots of Fig. 7. The lower aggregated power consumption constrained the system's ability to utilize the droop control mechanism for frequency regulation. As illustrated in the upper plot of Fig. 7, the system with higher hot water consumption outperformed the one with lower consumption in terms of frequency regulation. Furthermore, the lower plot of Fig. 7 demonstrates that higher hot water demand allowed for better adjustments in aggregated power consumption, enabling the system to store and release power more effectively for frequency stabilization.

These findings highlight the critical dependency of DR potential on the temporal statistics of hot water demand and the corresponding ON device population. However, sustained contributions diminished over time in both systems due to an increasing fraction of devices transitioning to the ON state, as shown in the middle plot of Fig. 7. This elevated demand not only correlated with a larger number of ON devices but also increased overall power consumption to maintain water temperatures, thereby limiting the permissible power range for DR.

Simulations further emphasized the importance of balancing

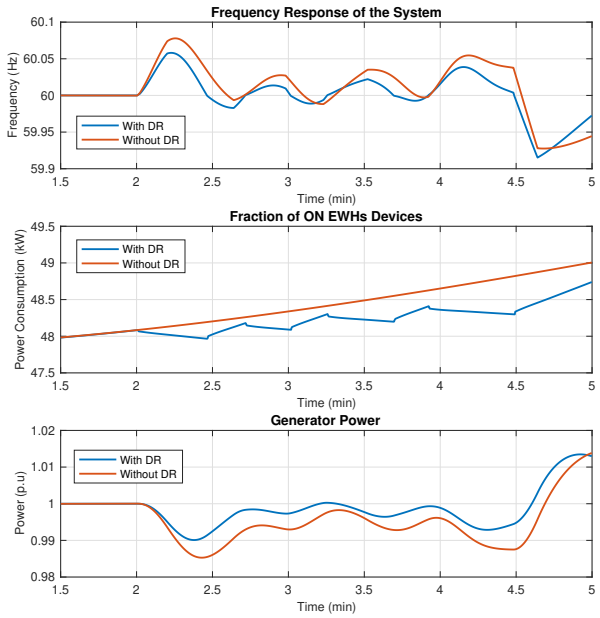

Fig. 6. System response to oscillatory perturbations with and without EWH-based DR. The upper plot shows the system frequency tracking performance, with EWHs improving the mean frequency. The middle plot illustrates the sinusoidal variation in the total number of ON devices, reflecting the droop mechanism's dynamic power adjustments. The lower plot highlights the reduced burden on generators, with the mean generator power staying closer to the nominal value of 1 p.u.

the number of ON devices to maximize frequency regulation efficacy. For instance, during a sudden generation loss of 0.015 p.u., the power change achieved with $A = 0.32\,^{\circ}\mathrm{C/min}$ was approximately 0.004 p.u., significantly less than the 0.015 p.u. achieved with $A = 0.81\,^{\circ}\mathrm{C/min}$. This underscores the strong correlation between hot water extraction rates and the aggregated power available from EWHs for DR. These results suggest that the choice of droop power thresholds and supplementary control mechanisms, such as predictive adjustments for anticipated demand peaks, could further optimize system performance.

Finally, simulations underscore the need to perform tests at various times of the day to capture the dynamic relationship between hot water demand, ON device fraction, and power availability for DR. Even with a reduced number of ON devices, DR remains effective in mitigating oscillatory load or generation perturbations, demonstrating the versatility of EWHs as a DR tool.

D. Extended Heating Modes and Temperature Thresholds

To address prolonged frequency deviations and enhance grid stability, a novel control scheme for EWHs was developed. This scheme enables devices to temporarily lower their set-point temperature during critical grid conditions, leveraging the thermal inertia of EWHs to significantly reduce power consumption while maintaining sufficient thermal storage to ensure user comfort.

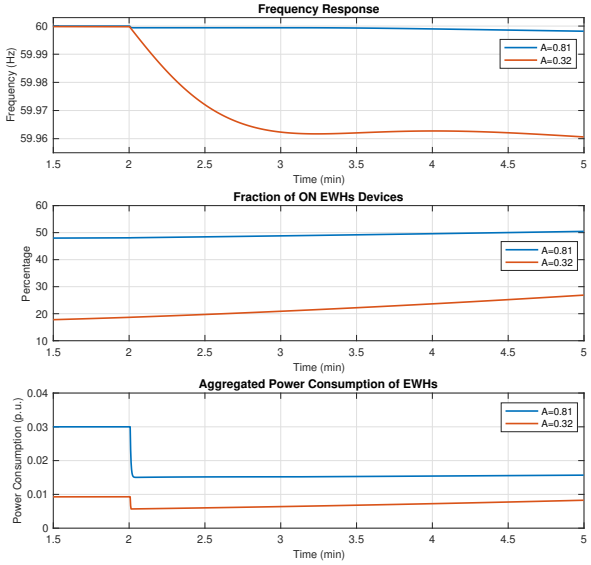

Fig. 7. Comparison of system performance under varying hot water demands. The upper plot shows frequency regulation, the middle plot shows the fraction of ON devices, and the lower plot illustrates aggregated power consumption.

The proposed strategy introduces a two-layer ON density model for EWHs, replacing the single ON layer used in previous configurations. Devices in the primary ON state ($m = 1$) reduce their power consumption proportionally to the magnitude of frequency deviation. This adjustment is governed by the droop-based mechanism discussed in Section II-C, enabling decentralized and autonomous operation. When the water temperature of these devices drops below a newly defined threshold (T_{sp}), typically set lower than the previous threshold ($T\_$), they transition to a secondary ON state ($m = 2$). In this state, devices operate at maximum power to restore water temperatures to a safe and acceptable range.

The transitions between these states are modeled using a hybrid-state Markov process, with updated PDFs to reflect the two-layer structure. Boundary conditions of the model were revised to accommodate the extended control framework, ensuring accurate representation of device behavior under the new scheme. Further details of these aspects are provided in Appendix B.

To evaluate the performance of the proposed control scheme, simulations were conducted under operational scenarios characterized by increased water demand and significant grid perturbations.

In one experiment, the control scheme was tested during a period of high hot water demand to assess its impact on system behavior. The surge in demand was simulated by setting $A = 81\frac{^{\circ}C}{\mathrm{min}}$, with the total power consumption of EWHs (P_{EWH}) at steady state initialized at 0.03 p.u. During this period, devices in layer $m = 1$ were allowed to reduce their power consumption to 10% of their nominal capacity. This reduction was implemented following the droop control

mechanism described in Section II-C when the grid frequency remained stable. Additionally, a perturbation of $+0.1$ p.u. was introduced, representing three times the nominal power consumption of EWHs. This scenario mimicked conditions with significant power surges on the grid.

Two systems were compared: one where EWHs operated under the traditional single ON layer framework, and another where the proposed setpoint change mechanism was activated. In the latter, devices were allowed to lower their thermostatic dead-band to $55°C$ once frequency deviations exceeded ± 0.1 Hz.

As shown in Fig. 8 upper plot, both systems exhibited similar frequency responses initially, as deviations remained within ± 0.1 Hz. However, once the frequency reached 59.9 Hz, the setpoint change mechanism significantly improved regulation by enabling EWHs to reduce their power consumption to $\frac{R'}{10}$, one-tenth of their nominal capacity.

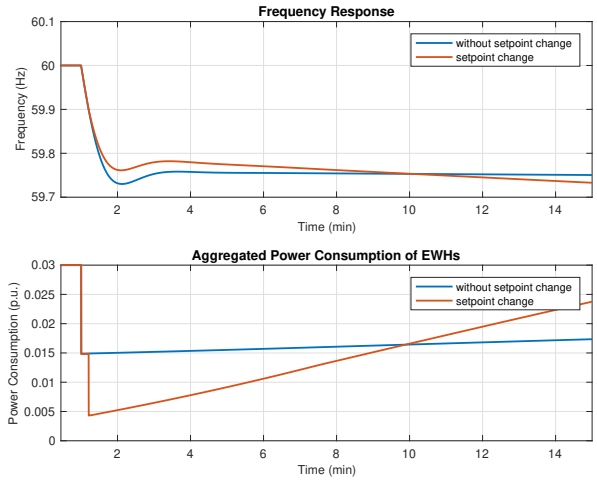

Fig. 8. Upper: Frequency responses of two systems with and without the setpoint change mechanism. The modified system showed better regulation beyond ± 0.1 Hz. Lower: Aggregated power consumption of EWHs and generation. Initial savings from the setpoint change decreased as more devices entered $m = 2$.

As the simulation progressed, more devices in the modified system transitioned to the secondary ON state ($m = 2$) to restore water temperatures, causing P_{EWH} to rise, as depicted in Fig. 9. While the setpoint change mechanism initially provided significant efficiency gains, its effectiveness diminished over time, highlighting a trade-off between immediate power savings and sustained operation.

These results demonstrate that under low water demand, less power is available for DR, but the system operates for a longer period, ensuring stability and reliability, illustrating in lower plot Fig. 8. Conversely, higher water demand allows for greater initial DR contributions but shortens the duration of effective operation. The simulations highlight the trade-offs between maximizing DR contributions and sustaining long-term system reliability under varying conditions.

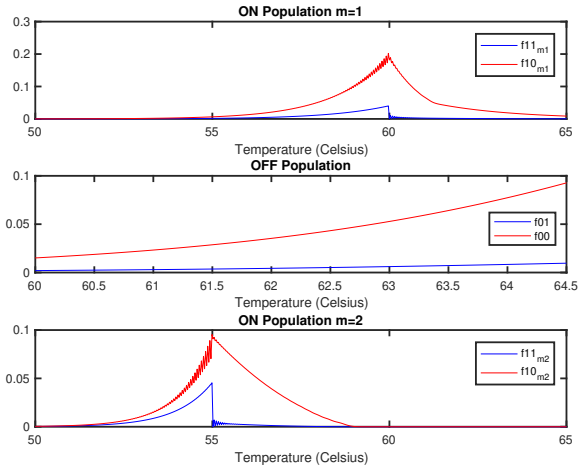

Fig. 9. Probability density functions updated by the Kolmogorov equations after 20 minutes of adjusting the EWH setpoint temperature to $T_{sp} = 55°\text{C}$. The EWHs fulfilled a shared energy demand, simulated with $A = 81°\text{C/min}$.

VI. Conclusion

This study introduces a decentralized droop-based control mechanism for EWHs to support grid frequency stabilization. By leveraging the thermal inertia and high energy consumption of EWHs, the proposed method enables rapid and autonomous adjustments in power consumption in response to frequency deviations.

Through detailed modeling using coupled PDEs and hybrid-state Markov processes, we demonstrated the effectiveness of EWHs in mitigating frequency fluctuations. Numerical simulations under various scenarios, including oscillatory perturbations and sudden load changes, showcased the ability of EWHs to improve frequency regulation by dynamically adjusting their power consumption and reducing the burden on traditional generation units.

While there have been numerous studies on the use of EWHs in demand response, the novel contribution of this work lies in the application of PDFs to analyze and predict the aggregate behavior of EWHs under frequency control. This approach provides a deeper understanding of the dynamic interaction between EWH populations and the power grid, allowing for more precise modeling of their contributions to grid stability.

The results also underscore the importance of temporal hot water consumption patterns, which significantly influence the available power range for demand response. Future research should explore integration with non-homogeneous EWH populations, predictive control for demand peaks, and cost-effectiveness analysis.

This work represents a significant advancement in the analytical tools available for demand response studies, offering a novel perspective on the utilization of EWHs to enhance grid resilience and efficiency.

ACKNOWLEDGMENT

The preferred spelling of the word “acknowledgment” in America is without an “e” after the “g”. Avoid the stilted expression “one of us (R. B. G.) thanks ...”. Instead, try “R. B. G. thanks...”. Put sponsor acknowledgments in the unnumbered footnote on the first page.

APPENDIX A
IDENTIFICATION OF MODEL PARAMETERS IN HOT WATER CONSUMPTION OF EWHS

For this study, a model for EWH was developed using the configuration parameters outlined in Table I.

The parameters a and R were derived using the following equations and the data from Table I:

$$a = \frac{UA_r}{MC_{pf}} = 0.193 \times 10^{-4}\,\frac{1}{\text{min}}, \tag{42}$$

$$R = \frac{R'}{MC_{pf}} = 0.2122\,\frac{^\circ C}{\text{min}\cdot \text{W}}. \tag{43}$$

Determination of Remaining Parameters

The remaining parameters A, α_0, and α_1 were determined using data on the average hourly hot water consumption (HWC) for a typical household, as shown in Fig. 10 [9]. A summary of the key parameters is provided in Table IV [14].

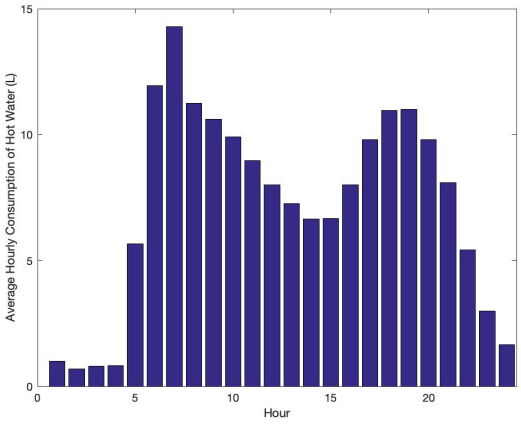

Fig. 10. Hourly household hot water consumption [14].

TABLE IV
HOT WATER CONSUMPTION PARAMETERS

Parameter (Name and Unit)	Value
Occupancy (Number of people)	3
Events (Hot water usage events per day)	21
Daily Water Demand (L)	201
Daily Energy Extraction (MJ)	16.7
Water Flow Rate ($\frac{\text{L}}{\text{min}}$)	5

The daily energy consumption relative to hot water usage is shown in Fig. 11.

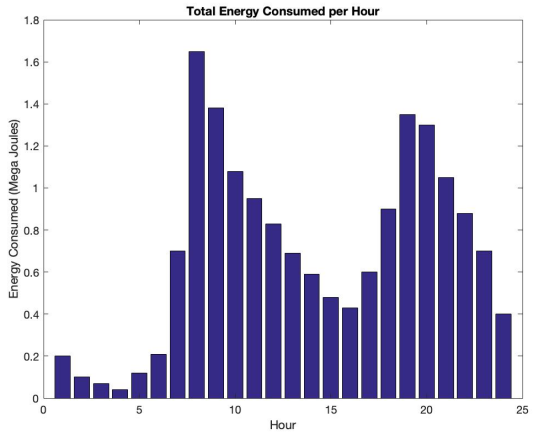

Fig. 11. Daily energy consumption relative to hot water usage in Fig. 10 [14].

Using the data in Tables I and IV, A and α_1 were calculated as:

$$A = \frac{\text{Daily Energy Extraction}}{\text{Event Time Span}} \cdot \frac{1}{\text{Tank Thermal Capacity}} = 0.3266\,\frac{^\circ C}{\text{min}}, \tag{44}$$

$$\alpha_1 = \frac{1}{\text{Duration of Water Event}} = \frac{21 \times 5}{201} = 0.52\,\text{min}^{-1}. \tag{45}$$

An hourly rate of energy extraction, based on Figures 10 and 11, is illustrated in Fig. 12. In Table II, the value of $A = 0.81\frac{^\circ C}{\text{min}}$ has been selected, representing the energy extraction rate around 9 PM. This time period is chosen due to the optimal number of ON EWHs, providing better leverage and insight into their behavior and contribution.

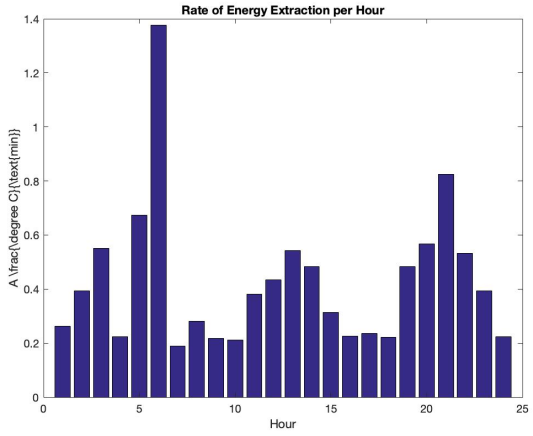

Fig. 12. Hourly rate of energy extraction based on Figures 10 and 11.

Parameter α_0

Using the steady-state fraction of ON devices (m_s) and the following equation [12]:

$$\bar{m} = \left(\frac{\alpha_1}{\alpha_1+\alpha_0}\right)\left[\frac{-\frac{\Delta}{r_{10}}}{-\frac{\Delta}{r_{10}}+\frac{\Delta}{r_{00}}}\right] + \left(\frac{\alpha_0}{\alpha_1+\alpha_0}\right)\left[\frac{-\frac{\Delta}{r_{11}}}{-\frac{\Delta}{r_{11}}+\frac{\Delta}{r_{10}}}\right] \quad (46)$$

where $\Delta = T_+ - T_-$, α_0 can be calculated. The values of m_s are obtained by dividing the hourly load in Fig. 11 by the maximum power of EWHs (4.5 kW). The results are listed in Table V.

TABLE V
AVERAGE POWER DEMAND BY EWH AND RESPECTIVE VALUES OF m_s AND α_0

Hour	**Load (kW)**	$\boldsymbol{m_s}$	$\boldsymbol{\alpha_0}$ (min^{-1})
0	0	0	0
1	0	0	0
2	0.018	0.04	0
3	0.033	0.007	0.001
4	0.26	0.058	0.009
5	1.14	0.252	0.042
6	0.746	0.166	0.028
⋮	⋮	⋮	⋮
23	0.147	0.033	0.005

APPENDIX B
PARTIAL DIFFERENTIAL EQUATIONS FOR THE NEW ON DENSITY LAYER IN MULTI LAYERS SYSTEM

The probability density functions for the new ON probability density layer, can be written with respect to the hybrid-state Markov process in a manner similar to the formulations for the other two density layers as discussed earlier in section III-C.

Probability Density Functions

The probability density functions for the new ON probability density layer are expressed as follows:

$$f'_{1j}(\lambda,t)d\lambda = P[\lambda \le T(t) \le \lambda + d\lambda, m(t)=2, q(t)=j], j=0,1 \quad (47)$$

Partial Differential Equations

The dynamics governing the new ON probability density layer $m = 2$ are given by the following partial differential equations:

$$\frac{\partial f'_{11}(\lambda,t)}{\partial t} = \frac{\partial}{\partial\lambda}[r'_{11}(\lambda,t)f'_{11}(\lambda,t)] - \alpha_1 f'_{11}(\lambda,t) + \alpha_0 f'_{10}(\lambda,t), \quad (48)$$

$$\frac{\partial f'_{10}(\lambda,t)}{\partial t} = \frac{\partial}{\partial\lambda}[r'_{10}(\lambda,t)f'_{10}(\lambda,t)] + \alpha_1 f'_{11}(\lambda,t) - \alpha_0 f'_{10}(\lambda,t). \quad (49)$$

Boundary Conditions

The following boundary conditions are specified for the new layer:

- **Conditions at infinity:**

$$f'_{11}(-\infty,t) = f'_{10}(-\infty,t) = 0. \quad (50)$$

- **Probability conservation:** At T_{sp}, for $j = 0, 1$:

$$r'_{1j}(T_{sp},t)f'^{b}_{1j}(T_{sp},t) + r_{1j}(T_{sp},t)f^{a}_{1j}(T_{sp},t) = 0. \quad (51)$$

- At T_-, for $j = 0, 1$:

$$-r_{1j}(T_-,t)f^{b}_{1j}(T_-,t) + r_{1j}(T_-,t)f^{c}_{1,j}(T_-,t) \quad (52)$$
$$+r_{0j}(T_-,t)f^{c}_{0j}(T_-,t) - r'_{1j}(T_-,t)f'^{c}_{1j}(T_-,t) = 0.$$

The absorbing boundaries added for $m = 2$ include:

- At T_-, for $j = 0, 1$:

$$0 \le -r'_{1j}(T_-,t)f'_{1j}(T_-,t). \quad (53)$$

- At T_{sp}, for $j = 0, 1$:

$$0 \le r'_{1j}(T_{sp},t)f'_{1j}(T_{sp},t). \quad (54)$$

Aggregate Behavior

The aggregate fraction of ON devices across all density layers is given by:

$$\bar{m}(t) = \mathbb{E}_w[m(t)] = \int_{-\infty}^{\infty}[f_{11}(\lambda,t) + f_{10}(\lambda,t) + f'_{11}(\lambda,t) + f'_{10}(\lambda,t)]d\lambda. \quad (55)$$

An illustration for understanding the regions and the way probability density functions look like has been provided in Fig 13.

REFERENCES

[1] P. Kundur, *Power System Stability and Control*, 2nd ed. New York: McGraw-Hill, 1994.

[2] F. C. Schweppe, R. D. Tabors, and J. L. Kirtley, "Homeostatic control for electric power usage: A new scheme for putting the customer in the control loop would exploit microprocessors to deliver energy more efficiently," *IEEE Spectrum*, vol. 19, no. 7, pp. 44–48, July 1982.

[3] Q.-C. Zhong, "Synchronized and democratized smart grids to underpin the third industrial revolution," *IFAC-PapersOnLine*, vol. 50, no. 1, pp. 3592–3597, 2017.

[4] J. Kondoh, N. Lu, and D. J. Hammerstrom, "An evaluation of the water heater load potential for providing regulation service," *IEEE Transactions on Power Systems*, vol. 26, no. 3, pp. 1309–1316, 2011.

[5] A. Sepulveda, L. Paull, W. G. Morsi, H. Li, C. P. Diduch, and L. Chang, "A novel demand side management program using water heaters and particle swarm optimization," in *2010 IEEE Electrical Power Energy Conference*, 2010, pp. 1–5.

[6] S. Pourmousavi and M. Nehrir, "Demand response for smart microgrid: Initial results," in *ISGT 2011*, 2011, pp. 1–6.

[7] A. Haider, W. Stark, and T. K. Brekken, "Electric hot water heater primary frequency control," in *2018 IEEE Energy Conversion Congress and Exposition (ECCE)*, 2018, pp. 2670–2675.

[8] M. Nehrir, R. Jia, D. Pierre, and D. Hammerstrom, "Power management of aggregate electric water heater loads by voltage control."

[9] J. Laurent and R. Malhame, "A physically-based computer model of aggregate electric water heating loads," *IEEE Transactions on Power Systems*, vol. 9, no. 3, pp. 1209–1217, 1994.

[10] Q. Shi, L. Yu, and Y. Xu, "Dynamic demand control for system frequency regulation: Concept review, algorithm comparison, and future vision," *Electric Power Systems Research*, vol. 154, pp. 154–162, 2018.

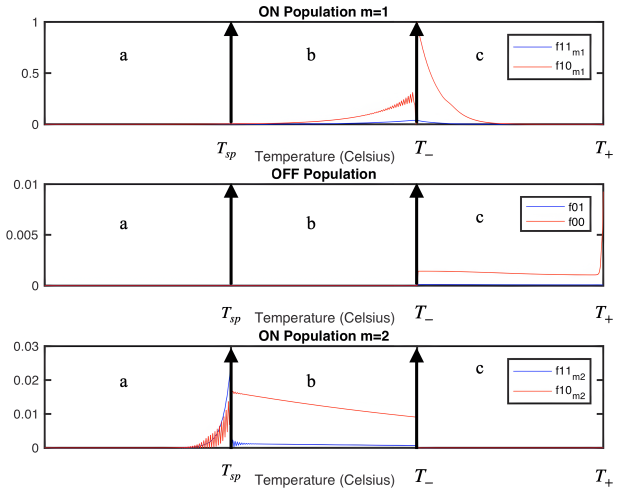

Fig. 13. Illustration of the dynamical system described by equations (9) to (12), and equations (48) to (49). The setpoint temperature T_{sp} is adjusted to lower the power consumption of the EWHs, aiming to conserve energy and compensate for generation deficits. Devices in $m = 1$ mode operate with reduced power consumption, lowering the water temperature to T_{sp}. Conversely, devices in $m = 2$ operate at maximum power to restore the water temperature to T_{-}, after which they switch back to $m = 1$ mode.

[11] R. Malhamé, "A markovian jump process-driven stochastic hybrid-state model, and its application for the prediction of the behavior of controlled electric water heating loads in power systems," in *Proc. 25th IEEE Conf. Decision Control*, 1986, pp. 1228–1230.

[12] R. Malhame, "A markovian jump process-driven stochastic hybrid-state model, and its application for the prediction of the behavior of controlled electric water heating loads in power systems," in *1986 25th IEEE Conference on Decision and Control*, 1986, pp. 1228–1230.

[13] FNET/GridEye Consortium, University of Tennessee Knoxville, "Frequency recording of quebec interconnection during the disturbance of april 25th, 2023," 2023.

[14] M. Gholizadeh, "Simulation and optimization of hot water systems in residential households," *Energy*, vol. 100, pp. 30–42, 2016.